Journal of Zhejiang University-SCIENCE B (Biomedicine & Biotechnology)
ISSN 1673-1581 (Print); ISSN 1862-1783 (Online)
www.jzus.zju.edu.cn; www.springerlink.com
E-mail: jzus@zju.edu.cn

Bionic mechanical design and 3D printing of novel porous Ti6Al4V implants for biomedical applications*

Wen-ming PENG[1], Yun-feng LIU[†‡1], Xian-feng JIANG[†‡1], Xing-tao DONG[1], Janice JUN[2], Dale A. BAUR[2], Jia-jie XU[3], Hui PAN[4], Xu XU[5]

[1]*Key Laboratory of E&M (Zhejiang University of Technology), Ministry of Education & Zhejiang Province, Hangzhou 310023, China*
[2]*Department of Oral and Maxillofacial Surgery, School of Dental Medicine, Case Western Reserve University, Cleveland, OH 44106, USA*
[3]*Head and Neck Surgery, Zhejiang Cancer Hospital, Hangzhou 310022, China*
[4]*Oral and Maxillofacial Surgery, Stomatology Hospital Affiliated to Zhejiang University School of Medicine, Hangzhou 310006, China*
[5]*Department of Stomatology, People's Hospital of Quzhou, Quzhou 324000, China*
[†]E-mail: liuyf76@126.com; xfjiang@zjut.edu.cn

Received Dec. 14, 2018; Revision accepted Mar. 13, 2019; Crosschecked June 15, 2019

Abstract: In maxillofacial surgery, there is a significant need for the design and fabrication of porous scaffolds with customizable bionic structures and mechanical properties suitable for bone tissue engineering. In this paper, we characterize the porous Ti6Al4V implant, which is one of the most promising and attractive biomedical applications due to the similarity of its modulus to human bones. We describe the mechanical properties of this implant, which we suggest is capable of providing important biological functions for bone tissue regeneration. We characterize a novel bionic design and fabrication process for porous implants. A design concept of "reducing dimensions and designing layer by layer" was used to construct layered slice and rod-connected mesh structure (LSRCMS) implants. Porous LSRCMS implants with different parameters and porosities were fabricated by selective laser melting (SLM). Printed samples were evaluated by microstructure characterization, specific mechanical properties were analyzed by mechanical tests, and finite element analysis was used to digitally calculate the stress characteristics of the LSRCMS under loading forces. Our results show that the samples fabricated by SLM had good structure printing quality with reasonable pore sizes. The porosity, pore size, and strut thickness of manufactured samples ranged from (60.95±0.27)% to (81.23±0.32)%, (480±28) to (685±31) μm, and (263±28) to (265±28) μm, respectively. The compression results show that the Young's modulus and the yield strength ranged from (2.23±0.03) to (6.36±0.06) GPa and (21.36±0.42) to (122.85±3.85) MPa, respectively. We also show that the Young's modulus and yield strength of the LSRCMS samples can be predicted by the Gibson-Ashby model. Further, we prove the structural stability of our novel design by finite element analysis. Our results illustrate that our novel SLM-fabricated porous Ti6Al4V scaffolds based on an LSRCMS are a promising material for bone implants, and are potentially applicable to the field of bone defect repair.

Key words: Layered slice and rod-connected mesh structure (LSRCMS); Porous Ti6Al4V implant; Bone defect repair; Selective laser melting (SLM); Mechanical properties; Finite element analysis
https://doi.org/10.1631/jzus.B1800622 **CLC number:** TH781

‡ Corresponding authors
* Project supported by the National Natural Science Foundation of China (No. 51775506), the Zhejiang Provincial Natural Science Foundation of China (No. LY18E050022), the Public Welfare Technology Application Research Project of Zhejiang Province (Nos. LGG19E050022 and 2017C33115), the Zhejiang Provincial Science & Technology Project for Medicine & Health (No. 2018KY878), and the Open Foundation of Zhejiang Provincial Top Key Discipline of Mechanical Engineering of Hangzhou Dianzi University, China
ORCID: Yun-feng LIU, https://orcid.org/0000-0001-8487-0078

1 Introduction

The repair of segmental bone defects is an important clinical problem in maxillofacial surgery. Autologous bone grafts and metal implants are commonly used in clinical reconstruction (Bose et al., 2013; Gepreel and Niinomi, 2013). However, autologous bone grafts have a limited source and are prone to complications such as infection. Reconstruction with metal implants can also lead to problems, including stress shielding and loosening in the postsurgical period (Qin et al., 2015). Therefore, both current methods of repairing segmental bone defects have significant drawbacks. An ideal implant with optimized parameters would be made of porous metal, and possess biological properties such as osseointegration and bone conduction. These properties are essential in the process of bone reconstruction and are currently considered some of the most attractive characteristics for biomedical implants (Attar et al., 2015; Wang et al., 2016).

As a novel concept for bone implant prostheses, porous implants have prospects for a wide range of applications and have attracted much attention. Porous implants with different porosities and mechanical properties, such as porous hip replacement femoral implants (Arabnejad et al., 2016, 2017), could mimic the structure of bone (Zhang et al., 2018). There are many methods for making porous implants, including powder sintering (Levine et al., 2006), frozen casting (Jung et al., 2013), and polymer sponge replacement (Jiang and He, 2014). However, these methods cannot precisely control the external shape of the implant or the internal void structure, nor guarantee the connectivity of internal pores. Compared to these methods, additive manufacturing technology or three-dimensional (3D) printing technology, and specifically, selective laser melting (SLM), can fabricate components with complicated geometries, and produce customized bone implants by accurately controlling the size, shape, and distribution of pores of the porous structure to achieve an optimal implant (Hazlehurst et al., 2014).

Previous research has involved experimental analysis of different types of titanium porous structures for biomedical applications (Yánez et al., 2018). At present, porous structures consist of two main forms: random geometric and regular cell structures. Random geometric structures tend to produce internal defects such as local deformation, while regular cell structures have a controllable uniform geometry with excellent mechanical properties (Kadkhodapour et al., 2015). A regular cell structure typically includes diamonds (Ahmadi et al., 2014), honeycombs (Ajdari et al., 2012), octahedrons (Sun et al., 2013), rhombic dodecahedrons (Horn et al., 2014), tetrakaidecahedrals (Zargarian et al., 2014), and lattices (Ravari et al., 2014). Recently, triply periodic minimal surfaces (TPMSs), as a promising approach, also have been studied and used in scaffold design (Yan et al., 2015; Bobbert et al., 2017; Ataee et al., 2018). Most of the research on regular cell structures focuses on the design of 3D crystal lattices obtained by periodic repetition of cell elements in all directions. However, the physiological structure of bone tissues is naturally heterogeneous and complex (Banse et al., 2001). Therefore, instead of attempting to reproduce the exact internal microarchitecture of bones, optimal scaffold design is focused on the creation of simplified models that are functionally similar to host bones in terms of their natural structure and mechanical properties (Giannitelli et al., 2014).

In light of the current challenges in the structural design and manufacturing of porous implants, we propose a novel structure made up of a layered slice and rod-connected mesh structure (LSRCMS) for titanium alloy implants, which resembles natural bone in both its structural and mechanical properties. In this study, a group of samples were fabricated by SLM, and then tested for mechanical properties using compressive mechanical experiments and finite element analysis. The implant structures with parameters most closely matching the mechanical properties of human bone tissue were determined by analyzing printed samples with different pore diameters and porosities by scanning electron microscope (SEM).

2 Materials and methods

2.1 Porous structure design

In view of the insufficiencies of traditional porous structures designed using 3D crystal lattices, this paper proposes the concept of "reducing dimensions, designing layer by layer" and transforms the design from a 3D lattice into a two-dimensional (2D) surface

grid (Fig. 1). Given that hexagonal holes have been shown to have higher biological activity than triangular or rectangular holes (van Bael et al., 2012), Rhinocero (Robert McNeel & Associates, USA) was used to design hexagonal grid cells of different sizes to form gradient porous structures. Each layer was staggered to avoid a "through-hole" structure, which affects the attachment of cells and passage of nutrients

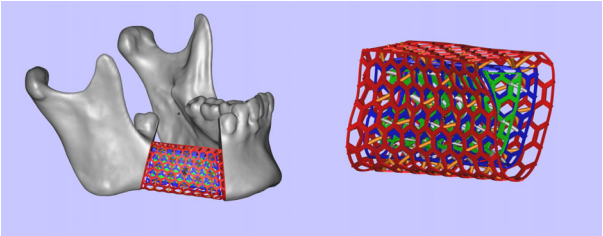

Fig. 1 Representative image of a "reduced dimensions, layered design"

(Fig. 2a). The external portion of the porous structure is compact and similar to cortical bone, and the internal portion is a sparse porous structure similar to cancellous bone. The distance (D_i, i=1, 2, …) between adjacent layers can be adjusted according to the thickness of the cortical bone and cancellous bone. Adjacent layers are connected at each node of the hexagon by connecting rods (Fig. 2b). The parameters of the connecting rods, including their direction and diameter, can be adjusted according to load on the implants to optimize the distribution of mechanical properties. This layout can be designed as a simple spatial 3D structure (Fig. 2c) or as a complex spatial curved structure (Fig. 2d), both of which are LSRCMS structures.

To analyze the mechanical properties of LSRCMS of different sizes, six groups of compression test specimens were designed with circular or rectangular pillar sections and with pores of 500, 600,

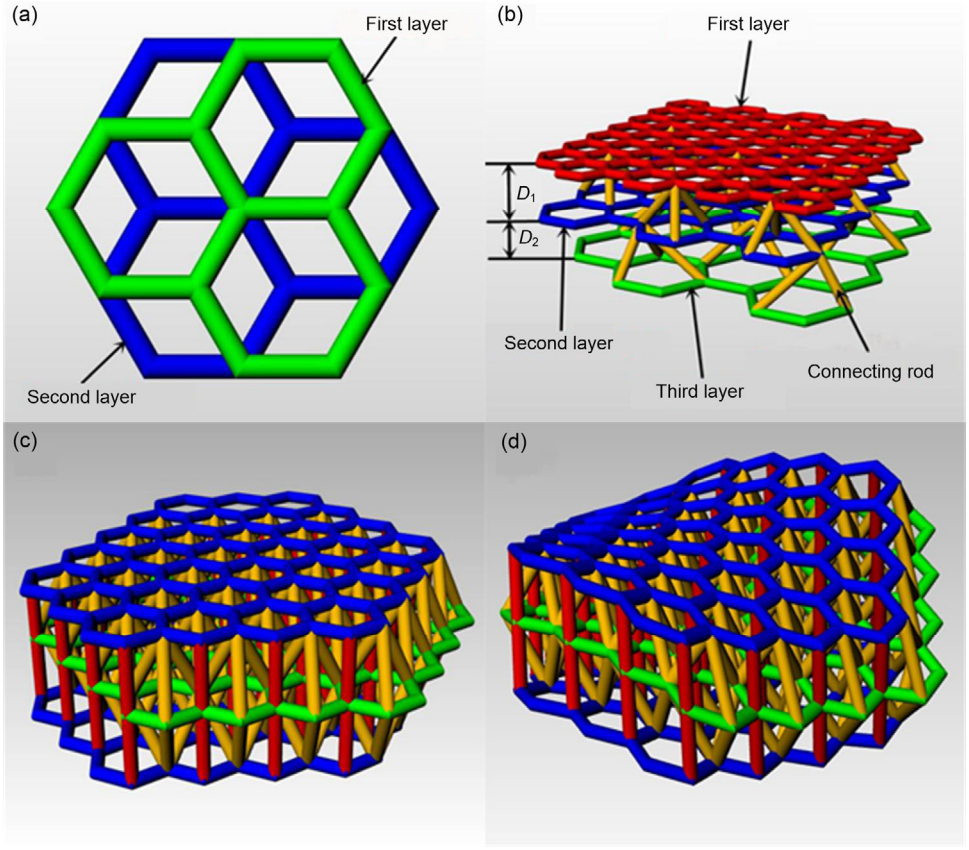

Fig. 2 Images of the layered slice and rod-connected network structures

(a) Positional relationship of adjacent layers; (b) Structural characteristics of the layered slice and rod-connected mesh structure (LSRCMS); (c) Spatial 3D structure; (d) Complex spatial curved structure

or 700 μm, named C500, C600, C700 and R500, R600, R700, respectively. The diameter of each connecting rod was 200 μm, and the distance between adjacent layers was 1 mm.

2.2 LSRCMS manufacturing

LSRCMS samples were fabricated using an SLM machine (Renishaw AM250), and Ti6Al4V powders with a diameter of 15–50 μm were printed in an argon-filled environment. A satisfactory printing result depended on appropriate parameters, such as laser power of 200 W, point distance of 75 μm, thickness of 50 μm, exposure time of 50 μs, and laser diameter of 75 μm. Three samples were fabricated for each group.

The post-processing steps of the printed samples included removal of the support and sandblasting, but because the surface still contained some metal particles, all samples were also cleaned in an ultrasonic cleaner with anhydrous ethanol for 15 min.

2.3 LSRCMS characterization

The pore diameters and strut sizes of the six groups of test samples were observed in all directions using optical microscopes (VW-6000E, Keyence, Japan). The microscopic surface morphology before deformation and the fractured surface morphology after deformation were observed using an SEM (VEGA3 SBH, Tescan, Czech Republic). Samples were cleaned and dried before observation and measurement to ensure that the surfaces of the structures were clean and free from debris.

2.4 Mechanical performance test

To evaluate the mechanical properties such as the yield strength and elastic modulus of the LSRCMSs, an Instron 8850 tester (Instron, Britain) was used to perform compression tests in the displacement control mode with a cylindrical sample (20 mm in height and 10 mm in diameter). The specimens were compressed at a constant deformation rate of 1.8 mm/min at room temperature (ISO 13314:2011 (International Organization for Standardization, 2011)), and the macroscopic deformation process was recorded during the compression process. Average values of the stress-strain curve obtained by experimental measurement were used to analyze the compression characteristics of the samples.

2.5 Finite element analysis

To simulate the weakness of the LSRCMSs under pressure, and to analyze and verify the mechanical properties of the porous structures comprehensively, finite element analysis of the designed structures was performed using ABAQUS (v6.14, Dassault Systèmes, Cedex, France) (Fig. 3). Simplified samples rather than standard cylindrical compressed samples were modeled and computationally analyzed to simplify the analysis process. The simplified samples had the same structure and pillar diameter as standard cylindrical compressed samples (height 8 mm; diameter 4 mm). The analyzed model had a ten-node tetrahedral mesh, and the material properties (elastic modulus (E) and Poisson's ratio (μ)) were set to E= 110 GPa, μ=0.3. To simulate the boundary conditions of the compression test, the bottom boundary conditions were set to be completely fixed and a force, which was consistent throughout the study, was loaded on the upper side (Smith et al., 2013).

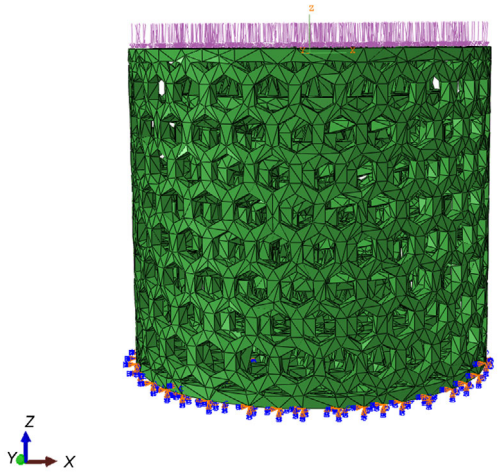

Fig. 3 Finite element model load and boundary conditions

3 Results

3.1 Pore structure characterization

Fig. 4 shows the LSRCMS sample fabricated by SLM, in which Fig. 4a shows an enlarged view of the overall porous structure. The pores of the structure assumed a hexagonal shape. The scaffold was a porous network with a hierarchical structure and mutually intersecting pores, and displayed excellent pore interconnectivity (Figs. 4c and 4d). Harrysson et al.

(2008) designed three kinds of structural implants, including mesh, hole, and solid, and found that mesh implants had a more uniform stress distribution and could effectively reduce stress shielding. Interconnected pore structures play an important role in the biocompatibility of porous biomaterials, which is one of the key factors for tissue ingrowth. Compared to through-hole structures, mesh pores are more conducive to the ingrowth and replication of cells, and structures with high porosity contribute to body fluid transport and bone ingrowth (Chen et al., 2017; Henriksson et al., 2017). Thus, the LSRCMS meets the requirements necessary for bone repair and growth.

Fig. 5 shows optical microscope (OM) and SEM images of SLM-fabricated LSRCMS samples. The pores and struts of each sample were measured by light microscopy, and the pore size and strut size distributions of various specifications were relatively uniform (Fig. 5a and Table 1). There were no fractures or cracks in the pillars, and continuity was good. We also found no defects at the connections between the layers and connecting rods within this complex structure, indicating that fabrication by SLM could preserve the characteristics of the CAD (computer aided design) model well. However, SEM observation (Fig. 5b) showed differences between the design size and the actual size due to powder adhering to the pillars, which affected their surface quality. After ultrasonic cleaning and sandblasting, few unmolten particles were observed, showing that vertical pillars have better surface quality than inclined pillars as in previous studies (Yavari et al., 2015). Although powder adhesion during SLM printing is an unavoidable side effect, the amount of adherent powder can be reduced by controlling the process parameters and optimizing the scanning method.

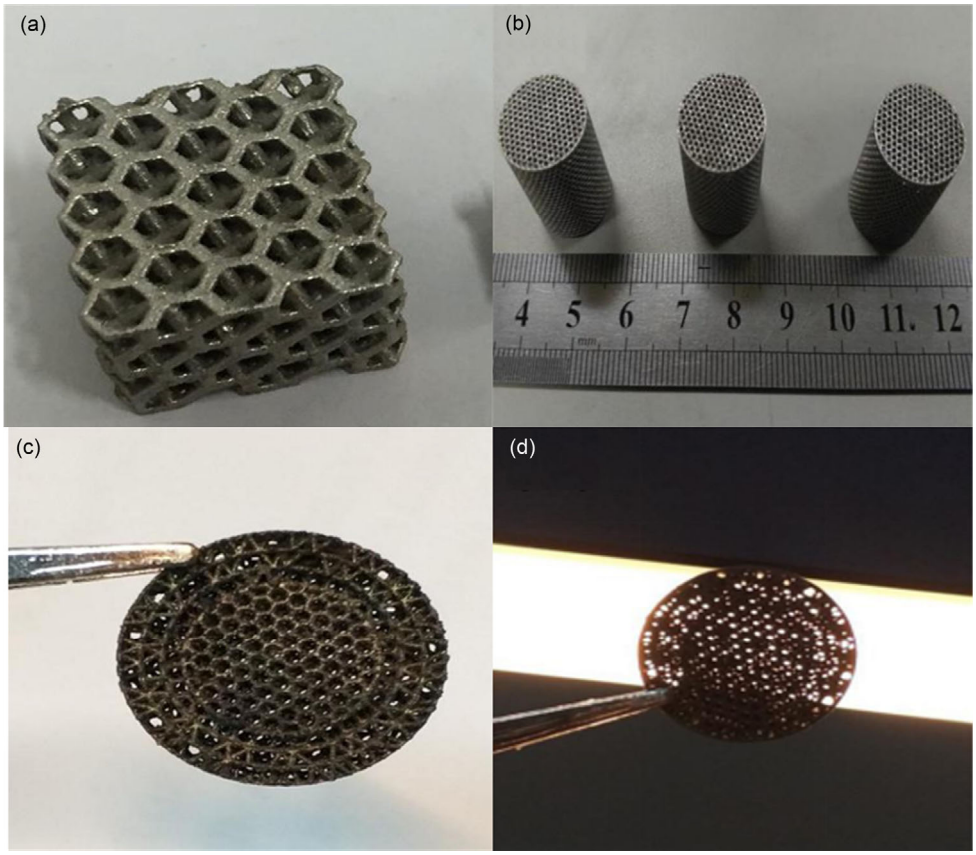

Fig. 4 Selective laser melting (SLM) printing of a Ti6Al4V porous structural specimen
(a) Magnified image of a porous structural unit; (b) Standard porous specimens prepared for a mechanical properties test; (c) Internal structure of a porous specimen; (d) Internal pores of a porous specimen

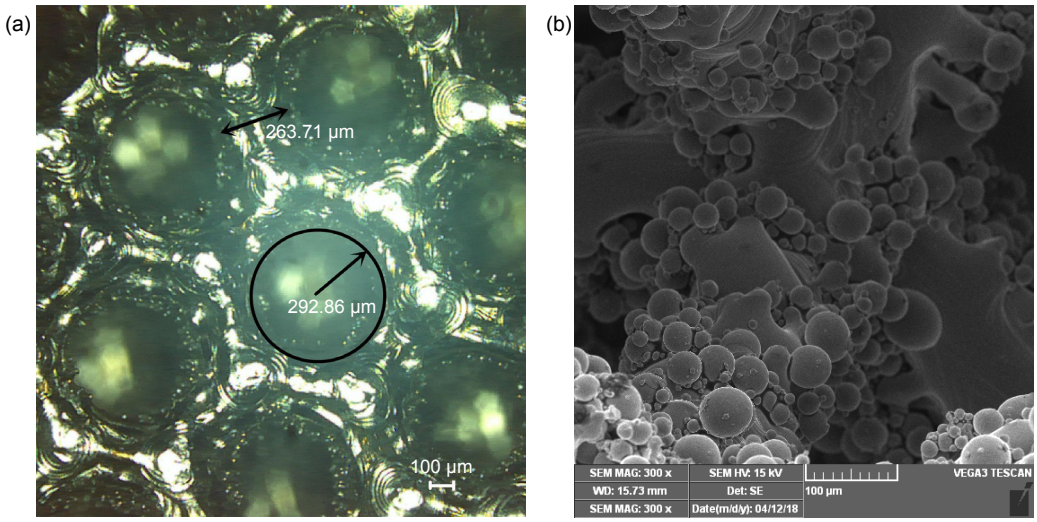

Fig. 5 Images of layered slice and rod-connected mesh structure (LSRCMS) characterization

(a) Optical microscope (OM) image of surfaces in the horizontal plane; (b) Scanning electron microscope (SEM) image of the surfaces of shaped pillars

Table 1 Pore structure parameters and mechanical properties of the Ti6Al4V specimen

Sample	Porosity (%)	Pore size (μm)	Strut size (μm)	Young's modulus: E (GPa)	Compressive strength: σ (MPa)
C700	81.23±0.32	683±30	263±28	2.23±0.03	22.57±0.43
C600	70.36±0.29	584±27	263±31	3.62±0.03	48.36±1.87
C500	62.75±0.30	480±28	264±30	6.06±0.05	122.85±3.85
R700	80.06±0.27	685±31	263±29	2.56±0.02	21.36±0.42
R600	69.55±0.30	581±30	264±31	3.89±0.03	45.69±1.79
R500	60.95±0.27	483±29	265±28	6.36±0.06	120.26±3.97

3.2 Mechanical behavior analysis

Table 1 lists the Young's modulus and compressive strength of the LSRCMS samples measured by uniaxial compression tests. For both cross-sectional structures, the elastic modulus and compressive strength of the samples decreased with increasing porosity. Compared to the rectangular structure, the circular structure had a lower elastic modulus and compressive strength. Melancon et al. (2017) stated that the elastic modulus of a bone implant should be adapted to the natural bone to avoid "stress shielding," and that the yield stress of the porous implant should be close to that of bone tissue. The elastic modulus of the circular cross-section structure C700 (pore diameter of 700 μm) was (2.23±0.03) GPa and the compressive strength was (22.57±0.43) MPa, which is equivalent to the mechanical properties of trabecular bone and cortical bone, indicating that this structure meets the mechanical property requirements of bone implants.

The stress-strain curve of the LSRCMS samples obtained by compression testing is shown in Fig. 6. Unlike traditional porous structure scaffolds, the LSRCMS showed a special deformation behavior in the compression process: a linear elastic deformation characterized by an elastic modulus occurred, followed by a yield-consolidation stage of local pillar fracture, further linear elastic deformation, local pillar breakage in the yield-compression stage, and finally the overall densification process of the complete structural yield platform. The structural collapse of the LSRCMS exhibited three distinct regions, differing from that of homogeneous porous scaffolds. According to the work of Han et al. (2018), our results illustrate that the LSRCMS has advantages in regard to mechanical properties and energy absorption.

Fig. 7 shows shallow dents and cleavage planes on the fracture surface and noticeable ductile dimples, which means that the LSRCMS has greater ductile

strength than a homogeneous porous scaffold. The macroscopic compressive deformation response of the LSRCMS was recorded on video, and Fig. 8 is a freeze frame from the video. LSRCMS samples with different parameters exhibited the same deformation characteristics. Firstly, a crush zone was established at the top of the sample (Fig. 8a). As the compression progressed, the crush zone continued to extend downward and gradually expanded (Figs. 8b and 8c). At the end, the specimen ruptured (Fig. 8d). Once the crush zone formed, cracks appeared in the micropores. The crack was in an axially diagonal position from the micro-hole. This process is consistent with the characteristics of the stress-strain curve, which indicates that the LSRCMS maintains good structural characteristics under pressure, and that no overall collapse phenomenon occurs during deformation.

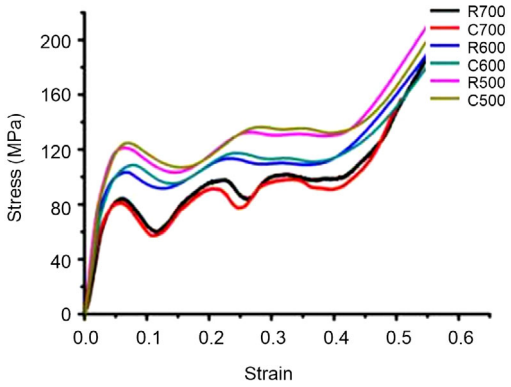

Fig. 6 Stress-strain curves obtained from compression tests of samples

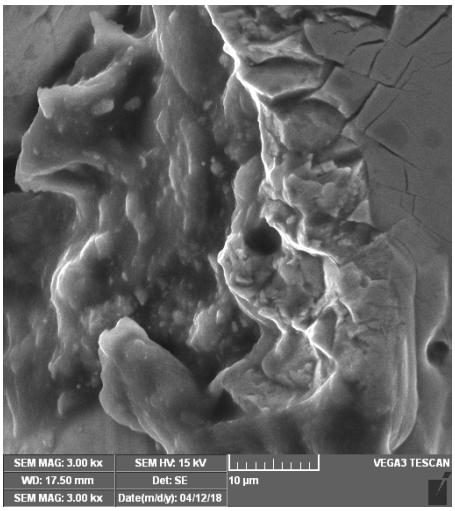

Fig. 7 SEM image of a compression fracture

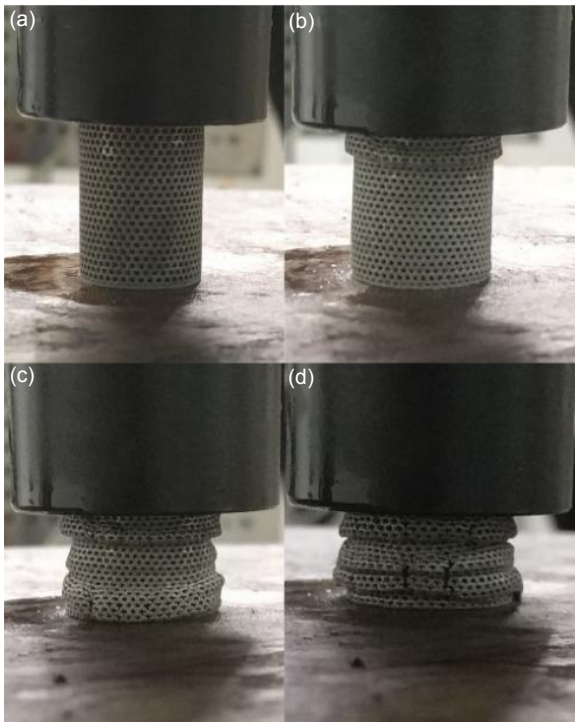

Fig. 8 Uniaxial compression of porous mesh structure at strains of 0% (a), 20% (b), 45% (c), and 60% (d)

3.3 Finite element analysis

Fig. 9 shows the results of the finite element analysis of the LSRCMS. From the stress distribution diagram, the stress at the rod shows a higher numerical response, which indicates that the stress distribution and concentration degree in the LSRCMS are embodied in the connecting rods. Each pillar in the LSRCMS remains in the elastic state, which is inconsistent with the results of Kadkhodapour et al. (2014, 2015) which indicated that stress concentration appeared around the node. The simulation results also showed that with the LSRCMS, forces could gradually be transferred from the loading area to different levels of layered slices by transmission through the connecting rods. Therefore, the LSRCMS can transmit load through its connecting rods to the overall structure, rather than bear the load in a local area or on a single node, which is consistent with the results of the compression test.

4 Discussion

The proper structure of scaffolds is an essential factor for satisfactory clinical outcomes of implants

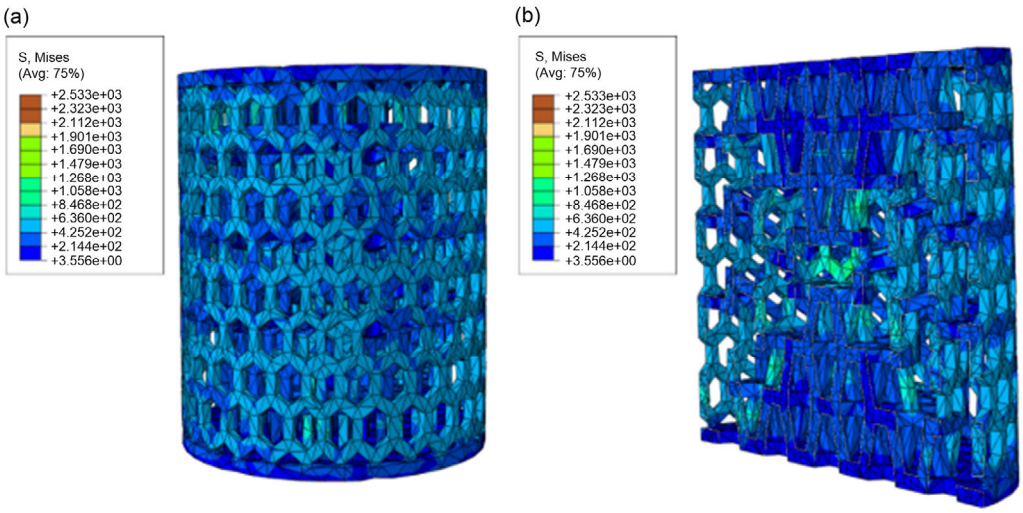

Fig. 9 Finite element analysis result for the layered slice and rod-connected mesh structure (LSRCMS)
(a) Overall structure; (b) Section view

(Surmeneva et al., 2017). Bone tissue is a 3D entity with a non-uniform structure, meaning that the ideal implant would be composed of a layered structure similar to that of bone tissue on multi-directional scales. Furthermore, the implant should have appropriate biological and biomechanical properties that are similar to those of the host bone and surrounding tissue. The internal pores of most porous scaffolds today are identical, which is contrary to the structure of real bone (Bernard et al., 2013), and it is difficult to guarantee the accuracy of the complex geometry and the continuity of implants in specific positions (Wang et al., 2016). In this study, we demonstrated that the LSRCMS has the potential to mimic human natural bone tissue by means of a customized layered structure, which is more appropriate for bone cell ingrowth.

Contrary to the failure of a traditional homogeneous porous scaffold, a different failure mechanism occurred in the LSRCMS. Beginning with the proximal layer of the LSRCMS, the scaffold collapsed steadily and smoothly in a layer-by-layer sequence until the ultimate full failure. There was also an absence of the diagonal shear band commonly seen in homogeneous porous structures (Gorny et al., 2011; Gümrük et al., 2013). These differences are attributed to the fact that the connecting rods in each layer eliminate the large drop in strength associated with shear failure. Compared to the smooth fracture surface of homogeneous porous scaffolds (Choy et al., 2017), LSRCMS samples have noticeable ductile dimples, making them more ductile than traditional porous scaffolds and better suited for SLM manufacturing processes.

The mechanical properties of porous scaffolds are generally determined by the relative density of the structures. In theory, according to the Gibson-Ashby model (Gibson and Ashby, 1997), the simple relationship between the elastic modulus, yield strength, and relative density of open-cell scaffolds is:

$$E^*/E_s=C_1(\rho^*/\rho_s)^{n_1}, \quad (1)$$

$$\sigma^*/\sigma_s=C_2(\rho^*/\rho_s)^{n_2}, \quad (2)$$

where E_s, ρ_s, and σ_s are the elastic modulus, density, and yield strength of fully dense solid materials, respectively, and E^*, ρ^*, and σ^* are the actual modulus, density, and yield strength of the porous structure, respectively. C_1 and C_2 are constants. For the ideal stochastic open cell form, the C_1 and C_2 constants are set to 1 and 0.3, respectively, in the Gibson-Ashby model. n_1 and n_2 are exponential factors.

Using Eqs. (1) and (2), the relationship was calculated with measured data (Fig. 10). Porous samples of three different porosities and two different cross-sections were manufactured by SLM, and their relative modulus, strength, and density were measured, with data analysis shown in Fig. 9. The results indicate that the relative modulus and density of the circular and rectangular sections followed a linear relationship with an exponential factor n_1 of 2.2 and

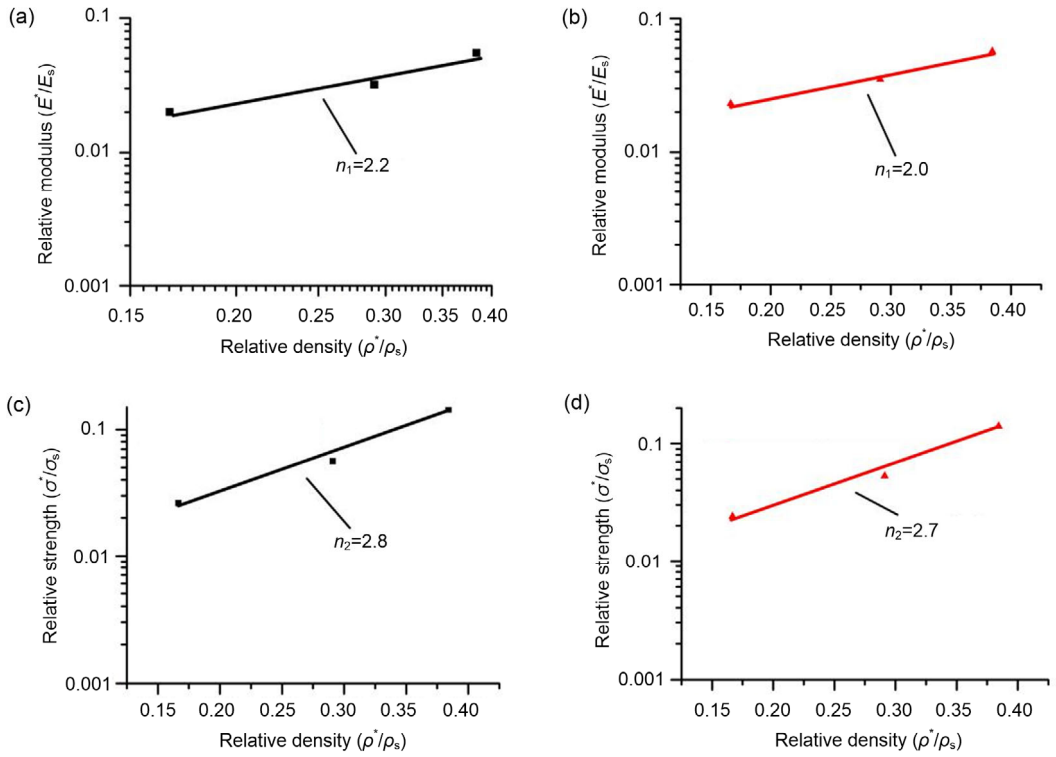

Fig. 10 Relative modulus and relative strength vs. relative density

(a) Relative modulus vs. relative density for the studied circle sections; (b) Relative modulus vs. relative density for the studied rectangular sections; (c) Relative strength vs. relative density for the studied circle sections; (d) Relative strength vs. relative density for the studied rectangular sections

2.0, respectively, and the relative strength and density followed a linear relationship with an exponential factor n_2 of 2.8 and 2.7, respectively, both of which are larger than the theoretically derived values of 1.5 for n_1 and 2.0 for n_2 in the Gibson-Ashby model. The reason for the difference is due mainly to the fact that the Gibson-Ashby model does not include the residual internal stress factors of the samples manufactured by the SLM processing technology, and the model is an ideal pillar structure. The irregular shape of the manufactured pillars is caused by powder adhesion of the SLM samples, subsequently altering their mechanical properties.

Although the intrinsic links between E^* and σ^* versus the relative density of the LSRCMS are not yet clear, the modulus, strength, and prediction data of the LSRCMS model have been consistent. Investigating the relationship between porous scaffold performance and structure has great potential in the field of biomedical science, and will help to design a structural model that can optimize the similarity of its mechanical properties to those of bone tissue.

The deformation of a porous structure fabricated by additive manufacturing technology is determined mainly by the morphological characteristics of the internal pore structure (Kadkhodapour et al., 2017), and the deformation of the pillar is determined mainly by the position of the pillar in the model. The pillars parallel to the direction of loading were dominated mainly by tensile deformation, and the inclined pillars with a certain angle to the direction of loading appeared mainly to have a bent deformation (Fig. 9). Therefore, compared to vertical pillars, inclined pillars can decompose the vertical downward force into oblique forces at the joints, where three inclined pillars at the same joint share the stress, which reduces the stress level within the pillars to some degree. Han et al. (2017) concluded that inclined struts can help to improve the mechanical properties of porous scaffolds. Smith et al. (2013) obtained similar results

through experiments and finite element analysis, showing that vertical pillars experience more stress than inclined pillar struts, and that during the deformation process, vertical pillars start to deform earlier than inclined pillars. Our finite element analysis result showed that connecting rods formed a 3D structure that can distribute the load through the overall structure, and that each rod can resist the external load. This provides a certain degree of flexibility and good distribution of force, which can improve the strength of the implant.

Li (2015) pointed out that the complete failure of a porous lattice structure fabricated by SLM is a result of the large number of slip bands, consisting of a tensile crack zone associated with tensile failure and a shear crack zone associated with compression failure. Compared to pillars, the SLM printing process of the LSRCMS created defects at nodes that were smaller and defects within the cross-sections that were larger. Therefore, the LSRCMS has sufficient mechanical properties to withstand higher stress levels at the nodes. Note that the above results were acquired mainly by simulating the stress distribution and deformation in a single compression process. To analyze the fatigue behavior of the LSRCMS model accurately, it is necessary to consider additional factors, including the irregularity of the pillar structures, the damage in the model, and the effect of crack propagation in the SLM process (Hedayati et al., 2016; Zargarian et al., 2016). Furthermore, it is necessary to evaluate the biological properties of the LSRCMS, including cell attachment, osseointegration, and bone growth within the structures. Also, animal experiments and physiological analysis should be conducted in the future.

5 Conclusions

In this study, SLM technology was used to create an LSRCMS scaffold with different porosities, which mimics the structures of human bone. The microstructure, mechanical response, and deformation process of the LSRCMS scaffold were investigated systematically. The findings were as follows:

(1) SEM and OM images showed that the novel implant structure of the LSRCMS could be fabricated successfully using SLM technology, with satisfactory design requirements, excellent connectivity of pores with fewer defects such as cracks, and good quality pillars.

(2) Compression tests showed that the LSRCMS had good mechanical response characteristics with an elastic modulus and yield strength within the ranges of 2.23–6.36 GPa and 21.36–122.85 MPa, respectively, which are consistent with the properties of bone tissue. Also, we showed that a circular pillar had better mechanical properties than a rectangular pillar. We further illustrated that SLM technology could produce high-strength and low-modulus titanium alloy porous implants.

(3) The relative modulus and relative strength of the LSRCMS were consistent with the Gibson-Ashby model, and the correlation indices of a circular cross-section and a rectangular cross-section were obtained. However, due to the specificity of the novel structure and for reasons specific to the SLM manufacturing process, the correlation index was larger than that of the original model.

(4) The results of finite element analysis showed that in the process of compression, the LSRCMS had good mechanical stability due to its structural flexibility and force transmission. Based on the different force deformation behaviors caused by differences in pillar direction and pore size, rod arrangements and pore sizes appropriate for future implant designs can be selected according to the loading conditions of the implant.

Contributors

Wen-ming PENG, Yun-feng LIU, and Xian-feng JIANG contributed to the study design and performed the statistical analysis. Wen-ming PENG, Janice JUN, and Dale A. BAUR drafted the manuscript. Jia-jie XU, Hui PAN, and Xu XU provided medical guidance and advice. Xing-tao Dong guided in 3D printing. All authors read and approved the final manuscript.

Compliance with ethics guidelines

Wen-ming PENG, Yun-feng LIU, Xian-feng JIANG, Xing-tao DONG, Janice JUN, Dale A. BAUR, Jia-jie XU, Hui PAN, and Xu XU declare that they have no conflict of interest.

This article does not contain any studies with human or animal subjects performed by any of the authors.

References

Ahmadi SM, Campoli G, Yavari SA, et al., 2014. Mechanical behavior of regular open-cell porous biomaterials made of

diamond lattice unit cells. *J Mech Behav Biomed Mater*, 34:106-115. https://doi.org/10.1016/j.jmbbm.2014.02.003

Ajdari A, Jahromi BH, Papadopoulos J, et al., 2012. Hierarchical honeycombs with tailorable properties. *Int J Solids Struct*, 49(11-12):1413-1419. https://doi.org/10.1016/j.ijsolstr.2012.02.029

Arabnejad S, Johnston RB, Pura JA, et al., 2016. High-strength porous biomaterials for bone replacement: a strategy to assess the interplay between cell morphology, mechanical properties, bone ingrowth and manufacturing constraints. *Acta Biomater*, 30:345-356. https://doi.org/10.1016/j.actbio.2015.10.048

Arabnejad S, Johnston B, Tanzer M, et al., 2017. Fully porous 3D printed titanium femoral stem to reduce stress-shielding following total hip arthroplasty. *J Orthop Res*, 35(8):1774-1783. https://doi.org/10.1002/jor.23445

Ataee A, Li YC, Fraser D, et al., 2018. Anisotropic Ti-6Al-4V gyroid scaffolds manufactured by electron beam melting (EBM) for bone implant applications. *Mater Design*, 137: 345-354. https://doi.org/10.1016/j.matdes.2017.10.040

Attar H, Löber L, Funk A, et al., 2015. Mechanical behavior of porous commercially pure Ti and Ti-TiB composite materials manufactured by selective laser melting. *Mater Sci Eng A*, 625:350-356. https://doi.org/10.1016/j.msea.2014.12.036

Banse X, Devogelaer JP, Munting E, et al., 2001. Inhomogeneity of human vertebral cancellous bone: systematic density and structure patterns inside the vertebral body. *Bone*, 28(5):563-571. https://doi.org/10.1016/S8756-3282(01)00425-2

Bernard S, Grimal Q, Laugier P, 2013. Accurate measurement of cortical bone elasticity tensor with resonant ultrasound spectroscopy. *J Mech Behav Biomed Mater*, 18:12-19. https://doi.org/10.1016/j.jmbbm.2012.09.017

Bobbert FSL, Lietaert K, Eftekhari AA, et al., 2017. Additively manufactured metallic porous biomaterials based on minimal surfaces: a unique combination of topological, mechanical, and mass transport properties. *Acta Biomater*, 53:572-584. https://doi.org/10.1016/j.actbio.2017.02.024

Bose S, Vahabzadeh S, Bandyopadhyay A, 2013. Bone tissue engineering using 3D printing. *Mater Today*, 16(12):496-504. https://doi.org/10.1016/j.mattod.2013.11.017

Chen SY, Huang JC, Pan CT, et al., 2017. Microstructure and mechanical properties of open-cell porous Ti-6Al-4V fabricated by selective laser melting. *J Alloys Compd*, 713: 248-254. https://doi.org/10.1016/j.jallcom.2017.04.190

Choy SY, Sun CN, Leong KF, et al., 2017. Compressive properties of functionally graded lattice structures manufactured by selective laser melting. *Mater Design*, 131: 112-120. https://doi.org/10.1016/j.matdes.2017.06.006

Gepreel MAH, Niinomi M, 2013. Biocompatibility of Ti-alloys for long-term implantation. *J Mech Behav Biomed Mater*, 20:407-415. https://doi.org/10.1016/j.jmbbm.2012.11.014

Giannitelli SM, Accoto D, Trombetta M, et al., 2014. Current trends in the design of scaffolds for computer-aided tissue engineering. *Acta Biomater*, 10(2):580-594. https://doi.org/10.1016/j.actbio.2013.10.024

Gibson LJ, Ashby MF, 1997. Cellular Solids: Structure and Properties, 2nd Ed. Cambridge University Press, Cambridge, UK, p.510.

Gorny B, Niendorf T, Lackmann J, et al., 2011. In situ characterization of the deformation and failure behavior of non-stochastic porous structures processed by selective laser melting. *Mater Sci Eng A*, 528(27):7962-7967. https://doi.org/10.1016/j.msea.2011.07.026

Gümrük R, Mines RAW, Karadeniz S, 2013. Static mechanical behaviours of stainless steel micro-lattice structures under different loading conditions. *Mater Sci Eng A*, 586:392-406. https://doi.org/10.1016/j.msea.2013.07.070

Han CJ, Yan CZ, Wen SF, et al., 2017. Effects of the unit cell topology on the compression properties of porous Co-Cr scaffolds fabricated via selective laser melting. *Rapid Prototyp J*, 23(1):16-27. https://doi.org/10.1108/RPJ-08-2015-0114

Han CJ, Li Y, Wang Q, et al., 2018. Continuous functionally graded porous titanium scaffolds manufactured by selective laser melting for bone implants. *J Mech Behav Biomed Mater*, 80:119-127. https://doi.org/10.1016/j.jmbbm.2018.01.013

Harrysson OLA, Cansizoglu O, Marcellin-Little DJ, et al., 2008. Direct metal fabrication of titanium implants with tailored materials and mechanical properties using electron beam melting technology. *Mater Sci Eng C Mater Biol Appl*, 28(3):366-373. https://doi.org/10.1016/j.msec.2007.04.022

Hazlehurst KB, Wang CJ, Stanford M, 2014. An investigation into the flexural characteristics of functionally graded cobalt chrome femoral stems manufactured using selective laser melting. *Mater Design*, 60:177-183. https://doi.org/10.1016/j.matdes.2014.03.068

Hedayati R, Hosseini-Toudeshky H, Sadighi M, et al., 2016. Computational prediction of the fatigue behavior of additively manufactured porous metallic biomaterials. *Int J Fatigue*, 84:67-79. https://doi.org/10.1016/j.ijfatigue.2015.11.017

Henriksson I, Gatenholm P, Hägg DA, 2017. Increased lipid accumulation and adipogenic gene expression of adipocytes in 3D bioprinted nanocellulose scaffolds. *Biofabrication*, 9(1):015022. https://doi.org/10.1088/1758-5090/aa5c1c

Horn TJ, Harrysson OLA, Marcellin-Little DJ, et al., 2014.

Flexural properties of Ti6Al4V rhombic dodecahedron open cellular structures fabricated with electron beam melting. *Addit Manuf*, 1-4:2-11. https://doi.org/10.1016/j.addma.2014.05.001

International Organization for Standardization, 2011. Mechanical Testing of Metals—Ductility Testing—Compression Test for Porous and Cellular Metals, ISO 13314:2011. International Organization for Standardization, Switzerland.

Jiang GF, He G, 2014. Enhancement of the porous titanium with entangled wire structure for load-bearing biomedical applications. *Mater Design*, 56:241-244. https://doi.org/10.1016/j.matdes.2013.11.019

Jung HD, Yook SW, Jang TS, et al., 2013. Dynamic freeze casting for the production of porous titanium (Ti) scaffolds. *Mater Sci Eng C Mater Biol Appl*, 33(1):59-63. https://doi.org/10.1016/j.msec.2012.08.004

Kadkhodapour J, Montazerian H, Raeisi S, 2014. Investigating internal architecture effect in plastic deformation and failure for TPMS-based scaffolds using simulation methods and experimental procedure. *Mater Sci Eng C Mater Biol Appl*, 43:587-597. https://doi.org/10.1016/j.msec.2014.07.047

Kadkhodapour J, Montazerian H, Darabi AC, et al., 2015. Failure mechanisms of additively manufactured porous biomaterials: effects of porosity and type of unit cell. *J Mech Behav Biomed Mater*, 50:180-191. https://doi.org/10.1016/j.jmbbm.2015.06.012

Kadkhodapour J, Montazerian H, Darabi AC, et al., 2017. The relationships between deformation mechanisms and mechanical properties of additively manufactured porous biomaterials. *J Mech Behav Biomed Mater*, 70:28-42. https://doi.org/10.1016/j.jmbbm.2016.09.018

Levine BR, Sporer S, Poggie RA, et al., 2006. Experimental and clinical performance of porous tantalum in orthopedic surgery. *Biomaterials*, 27(27):4671-4681. https://doi.org/10.1016/j.biomaterials.2006.04.041

Li PF, 2015. Constitutive and failure behaviour in selective laser melted stainless steel for microlattice structures. *Mater Sci Eng A*, 622:114-120. https://doi.org/10.1016/j.msea.2014.11.028

Melancon D, Bagheri ZS, Johnston RB, et al., 2017. Mechanical characterization of structurally porous biomaterials built via additive manufacturing: experiments, predictive models, and design maps for load-bearing bone replacement implants. *Acta Biomater*, 63:350-368. https://doi.org/10.1016/j.actbio.2017.09.013

Qin M, Liu YX, Wang L, et al., 2015. Design and optimization of the fixing plate for customized mandible implants. *J Craniomaxillofac Surg*, 43(7):1296-1302. https://doi.org/10.1016/j.jcms.2015.06.003

Ravari MRK, Kadkhodaei M, Badrossamay M, et al., 2014. Numerical investigation on mechanical properties of cellular lattice structures fabricated by fused deposition modeling. *Int J Mech Sci*, 88:154-161. https://doi.org/10.1016/j.ijmecsci.2014.08.009

Smith M, Guan Z, Cantwell WJ, 2013. Finite element modelling of the compressive response of lattice structures manufactured using the selective laser melting technique. *Int J Mech Sci*, 67:28-41. https://doi.org/10.1016/j.ijmecsci.2012.12.004

Sun JF, Yang YQ, Wang D, 2013. Mechanical properties of a Ti6Al4V porous structure produced by selective laser melting. *Mater Design*, 49:545-552. https://doi.org/10.1016/j.matdes.2013.01.038

Surmeneva MA, Surmenev RA, Chudinova EA, et al., 2017. Fabrication of multiple-layered gradient cellular metal scaffold via electron beam melting for segmental bone reconstruction. *Mater Design*, 133:195-204. https://doi.org/10.1016/j.matdes.2017.07.059

van Bael S, Chai YC, Truscello S, et al., 2012. The effect of pore geometry on the in vitro biological behavior of human periosteum-derived cells seeded on selective laser-melted Ti6Al4V bone scaffolds. *Acta Biomater*, 8(7):2824-2834. https://doi.org/10.1016/j.actbio.2012.04.001

Wang XJ, Xu SQ, Zhou SW, et al., 2016. Topological design and additive manufacturing of porous metals for bone scaffolds and orthopaedic implants: a review. *Biomaterials*, 83:127-141. https://doi.org/10.1016/j.biomaterials.2016.01.012

Yan CZ, Hao L, Hussein A, et al., 2015. Ti-6Al-4V triply periodic minimal surface structures for bone implants fabricated via selective laser melting. *J Mech Behav Biomed Mater*, 51:61-73. https://doi.org/10.1016/j.jmbbm.2015.06.024

Yánez A, Cuadrado A, Martel O, et al., 2018. Gyroid porous titanium structures: a versatile solution to be used as scaffolds in bone defect reconstruction. *Mater Design*, 140:21-29. https://doi.org/10.1016/j.matdes.2017.11.050

Yavari SA, Ahmadi SM, Wauthle R, et al., 2015. Relationship between unit cell type and porosity and the fatigue behavior of selective laser melted meta-biomaterials. *J Mech Behav Biomed Mater*, 43:91-100. https://doi.org/10.1016/j.jmbbm.2014.12.015

Zargarian A, Esfahanian M, Kadkhodapour J, et al., 2014. Effect of solid distribution on elastic properties of open-cell cellular solids using numerical and experimental methods. *J Mech Behav Biomed Mater*, 37:264-273. https://doi.org/10.1016/j.jmbbm.2014.05.018

Zargarian A, Esfahanian M, Kadkhodapour J, et al., 2016. Numerical simulation of the fatigue behavior of additive manufactured titanium porous lattice structures. *Mater Sci Eng C Mater Biol Appl*, 60:339-347. https://doi.org/10.1016/j.msec.2015.11.054

Zhang BQ, Pe X, Zhou CC, et al., 2018. The biomimetic design and 3D printing of customized mechanical properties porous Ti6Al4V scaffold for load-bearing bone reconstruction. *Mater Design*, 152:30-39. https://doi.org/10.1016/j.matdes.2018.04.065

中文概要

题　目：用于生物医学的新型多孔 Ti6Al4V 植入物的仿生设计和 3D 打印

目　的：多孔结构植入体在骨科修复领域具有极大的应用前景。本研究提出了一种在结构与力学性能方面更贴近人体骨组织的多孔 Ti6Al4V 植入体。

创新点：针对骨组织的结构特点，提出了“分层设计”理念，以期更好地模拟皮质骨和松质骨的结构。除了结构相似以外，这种植入体在力学性能和结构稳定性方面同样具有优势。

方　法：将传统多孔植入体三维晶胞设计方法转化为二维设计理念，设计出一种分层杆连接多孔结构，并利用选择性激光熔融（SLM）技术打印出样品；然后通过光学显微镜评测打印效果，利用单轴压缩试验研究分析样品的力学性能；最后利用有限元方法分析多孔结构的结构稳定性。

结　论：本研究所设计的新型分层杆连接结构可以通过 SLM 实现高质量的打印，且尺寸合理，力学性能与骨组织相接近，结构稳定性优于传统多孔结构。这种新型多孔结构植入体在骨缺损修复领域具有较好的潜在应用前景。

关键词：分层片状杆连接多孔结构（LSRCMS）；多孔 Ti6Al4V植入体；骨缺损修复；选择性激光熔融（SLM）；机械性能；有限元分析